Monthly Notices of the ROYAL ASTRONOMICAL SOCIETY LETTERS

Mon. Not. R. Astron. Soc. **401,** L24–L28 (2010) doi:10.1111/j.1745-3933.2009.00778.x

Wavelet-based Faraday rotation measure synthesis

P. Frick,[1⋆] D. Sokoloff,[2] R. Stepanov[1] and R. Beck[3]

[1]*Institute of Continuous Media Mechanics, Korolyov str. 1, 614013 Perm, Russia*
[2]*Department of Physics, Moscow University, 119899 Moscow, Russia*
[3]*Max-Planck-Institut für Radioastronomie, Auf dem Hügel 69, 53121 Bonn, Germany*

Accepted 2009 October 13. Received 2009 October 13; in original form 2009 July 7

ABSTRACT

The Faraday rotation measure synthesis, as a method for analysing multichannel observations of polarized radio emission to investigate galactic magnetic field structures requires the definition of complex polarized intensity in the wavelength range $-\infty < \lambda^2 < \infty$. The problem is that the measurements at negative λ^2 are not possible. We introduce a simple method for continuation of the observed complex polarized intensity $P(\lambda^2)$ into the domain $\lambda^2 < 0$ using symmetry arguments. The method is suggested in context of magnetic field recognition in galactic discs where the magnetic field is supposed to have a maximum in the equatorial plane. The method is quite simple when applied to a single Faraday rotating structure on the line of sight. Recognition of several structures on the same line of sight requires a more sophisticated technique. We also introduce a wavelet-based algorithm which allows us to consider a set of isolated structures in the (ϕ, λ^2) plane (where ϕ is the Faraday depth). The method essentially improves the possibilities for reconstruction of complicated Faraday structures using the capabilities of modern radio telescopes.

Key words: polarization – methods: data analysis – galaxies: magnetic fields.

1 INTRODUCTION

Observations of polarized radio emission are the main sources of information on magnetic fields of galaxies. The basic idea of magnetic field analysis from polarized radio emission data originates in the classical paper of Burn (1966) (for a later development see Sokoloff et al. 1998). In particular, Burn (1966) noted that the complex polarized intensity P obtained from a radio source is related to the Faraday dispersion function $F(\phi)$ as

$$P(\lambda^2) = \int_{-\infty}^{\infty} F(\phi) \mathrm{e}^{2\mathrm{i}\phi\lambda^2}\, \mathrm{d}\phi. \quad (1)$$

$F(\phi)$ is the fraction of radiation with the Faraday depth ϕ multiplied by intrinsic complex polarization and it is an important emission characteristic of interest. Here the Faraday depth ϕ is defined by

$$\phi(z) = -0.81 \int_{z}^{0} B_{\parallel} n_{\mathrm{e}}\, \mathrm{d}z', \quad (2)$$

where $B_{\parallel}$ is the line-of-sight magnetic field component measured in μG, n_{e} is the thermal electron density measured in cm^{-3} and the integral is taken from the observer at $z = 0$ over the region which contains both, magnetic fields and free electrons, and z is measured in parsecs. Following equation (1) P is the inverse Fourier transform of F. Correspondingly, the Faraday dispersion function F is the Fourier transform of the complex polarized intensity:

$$F(\phi) = \frac{1}{\pi} \hat{P}(k), \quad (3)$$

where $k = 2\phi$, and the Fourier transform is defined as

$$f(x) = \frac{1}{2\pi} \int_{-\infty}^{\infty} \hat{f}(k)\, \mathrm{e}^{\mathrm{i}kx} \mathrm{d}k, \quad \hat{f}(k) = \int_{-\infty}^{\infty} f(x)\, \mathrm{e}^{-\mathrm{i}kx}\, \mathrm{d}x. \quad (4)$$

Implementation of multichannel spectropolarimetry on modern radio telescopes provided observations of P over a wide range of λ (e.g. Haverkorn, Katgert & de Bruyn 2000) which made the use of equation (3) possible. This is the idea of Faraday rotation measure (RM) Synthesis (Brentjens & de Bruyn 2005) which opened new perspectives in investigations of magnetic field of galaxies and clusters of galaxies (Haverkorn, Katgert & de Bruyn 2003; de Bruyn & Brentjens 2005; Beck 2009; Heald, Braun & Edmonds 2009).

A key problem of RM Synthesis application is that P is defined only for $\lambda^2 > 0$ and in practice can be observed only in a finite spectral band. Moreover, the maximum of P in practice can be located outside the available spectral band (see e.g. Fig. 1b). Development of robust methods for the reconstruction of F from P in a given spectral range becomes crucial for the practical implementation of RM Synthesis.

Fig. 1 shows results of RM Synthesis applied to a standard test as exploited by Brentjens & de Bruyn (2005). Panel (a) shows the function F, which includes three *real-valued* box-like structures and panel (b) – the corresponding polarized intensity P (the dashed

⋆E-mail: frick@icmm.ru

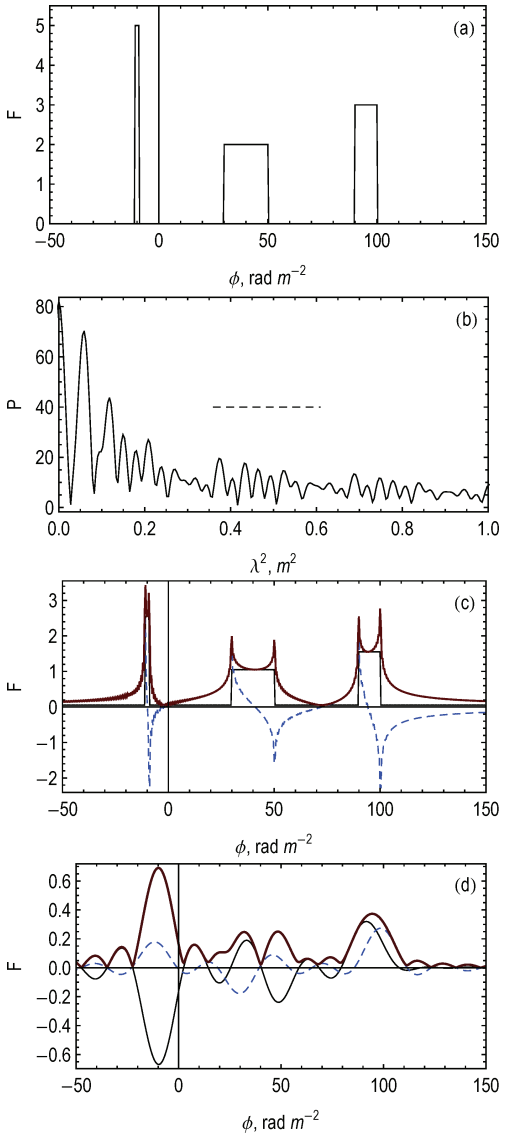

Figure 1. RM Synthesis reconstruction of a standard example from Brentjens & de Bruyn (2005): (a) initial $F(\phi)$ which is chosen purely real; (b) amplitude of $PI(\lambda^2)$; (c) $F(\phi)$ reconstructed with whole domain $\lambda^2 > 0$: real part – thin solid, imaginary part – dashed, amplitude – thick solid; (d) $F(\phi)$ reconstructed from the data of spectral band $0.6 < \lambda < 0.78$ m. The spectral window of observations is indicated in panel (b) by horizontal dashed line.

horizontal line shows the spectral window $0.6 < \lambda < 0.78$ m). We used a channel spacing of $\delta\lambda = 0.4$ cm. Hereafter, F and P are numerically evaluated in arbitrary but mutually consistent units. Note that F is in general a complex-valued function. Its modulus defines the emission and its phase defines the intrinsic position angle. Panel (c) shows the result of the straightforward application of the RM Synthesis algorithm to the physical range $\lambda^2 > 0$, while $P(\lambda^2)$ is set to zero for all negative λ^2. We see that the real part of the reconstructed signal is the same as the initial one (except that it has a twice lower amplitude); however, the reconstructed signal obtains a substantial imaginary part with a shape which is quite remote from the real part. This leads to a change of the emission distribution and a loss of any information concerning the position angle (apart from the central point of the emission region, where the position angle is correctly zero). In the context of chaotic magnetic fields in galaxy clusters this loss is less important (de Bruyn & Brentjens 2005), but in galactic magnetic field studies it becomes crucial because the intrinsic position angle determines the orientation of the regular magnetic field component perpendicular to the line of sight. Fig. 1d shows that the reconstruction becomes much more difficult if we restrict the data to a relatively narrow spectral band $0.6 < \lambda < 0.78$ m. We see that even the sign of the reconstructed real part can be wrong. In that case the algorithm for finite spectral band introduced by Brentjens & de Bruyn (2005) was used.

A general message obtained from Fig. 1 is that in order to envisage possible ways to get a practical implementation of RM Synthesis, one has to include some additional information based on the nature of the physical phenomena which provide the Faraday rotation. Here we concentrate our efforts on the problems associated with missing $P(\lambda^2)$ for $\lambda^2 < 0$.

2 IMPROVING THE RM SYNTHESIS ALGORITHM

The complex-valued intensity of polarized radio emission for a given wavelength,

$$P(\lambda^2) = \int_0^\infty \varepsilon(z) \mathrm{e}^{2\mathrm{i}\chi(z)} \mathrm{e}^{2\mathrm{i}\phi(z)\lambda^2} \, \mathrm{d}z, \tag{5}$$

is defined by the emissivity ε and the intrinsic position angle χ along the line of sight. Here z is the distance from observer to a point in the emitting region; the integral is taken over the whole emitting region. If the Faraday depth ϕ is a monotonic function of z (which means that z is a single-valued function of ϕ), we can define the Faraday dispersion function as a function of the Faraday depth

$$F(\phi) = \varepsilon(\phi) \mathrm{e}^{2\mathrm{i}\chi(\phi)} \left(\frac{\mathrm{d}\phi}{\mathrm{d}z} \right)^{-1}. \tag{6}$$

In the ideal case, reconstructing the Faraday dispersion function F from (3) and knowing the Faraday depth ϕ for any z, one can derive the characteristics of radio emission (ε and χ) along the line of sight. They can be used as a tomography in order to derive some characteristics of the magnetic field distribution from F. The task of RM Synthesis is much more modest and concerns the reconstruction of the Faraday function from the observed polarized emission which itself is already a complicated problem.

Let us consider a physically motivated simple example, i.e. P produced by a two-layer system, to isolate and overcome the shortcomings of the RM Synthesis technique. Each layer contains a homogeneous magnetic field which has non-vanishing line-of-sight and perpendicular components. Both layers are thought to be emitting and rotating polarized radio waves. The corresponding $F(\phi)$ is shown in Fig. 2(a). It is important for the discussion below that the analysed signal has non-vanishing real and imaginary parts. The absolute value of $F(\phi)$ indicates how much polarized emission comes from a region with the Faraday depth ϕ and its phase gives the intrinsic position angle (about 13° and 31°) of the emission. Just to illustrate the variety of possible situations, we choose two different shapes of the slabs, i.e. one slab with sharp boundaries and one with a Gaussian shape.

The result of the straightforward application of RM Synthesis where the integral is taken over the physically admissible region $\lambda^2 > 0$ is shown in Fig. 2(b). RM Synthesis reproduces to some extent the absolute value of the signal, but fails to reproduce its phase. A naive interpretation of this result could be that field reversals

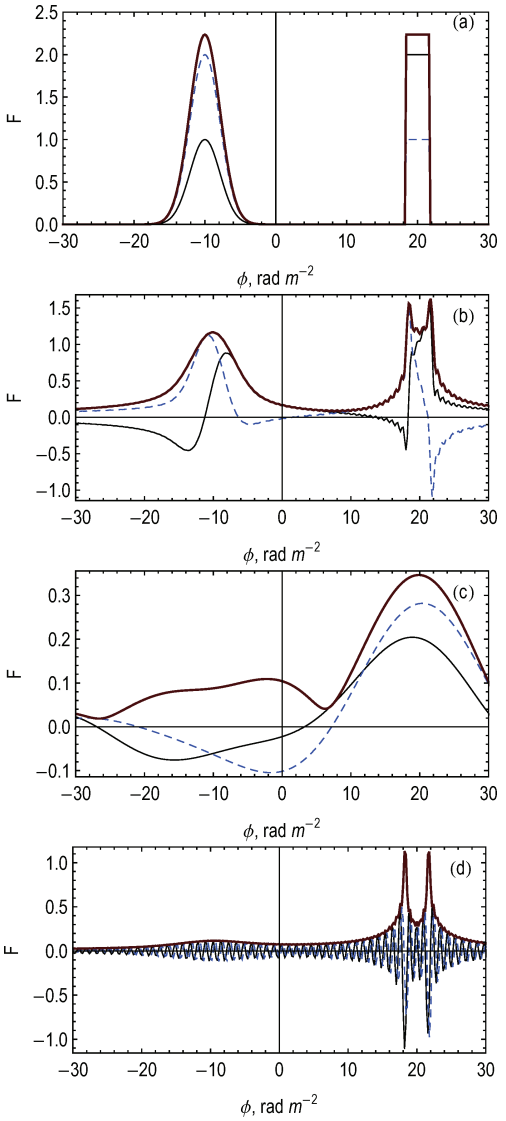

Figure 2. Standard RM Synthesis for a test Faraday dispersion function. (a) Original test function which includes one Gaussian and one box structure. Reconstructions: (b) using the whole domain $\lambda^2 > 0$; (c) using the window $0.6 < \lambda < 0.78$ m; (d) using the window $0.6 < \lambda < 2.5$ m. Real part – thin solid, imaginary part – dashed, amplitude – thick solid.

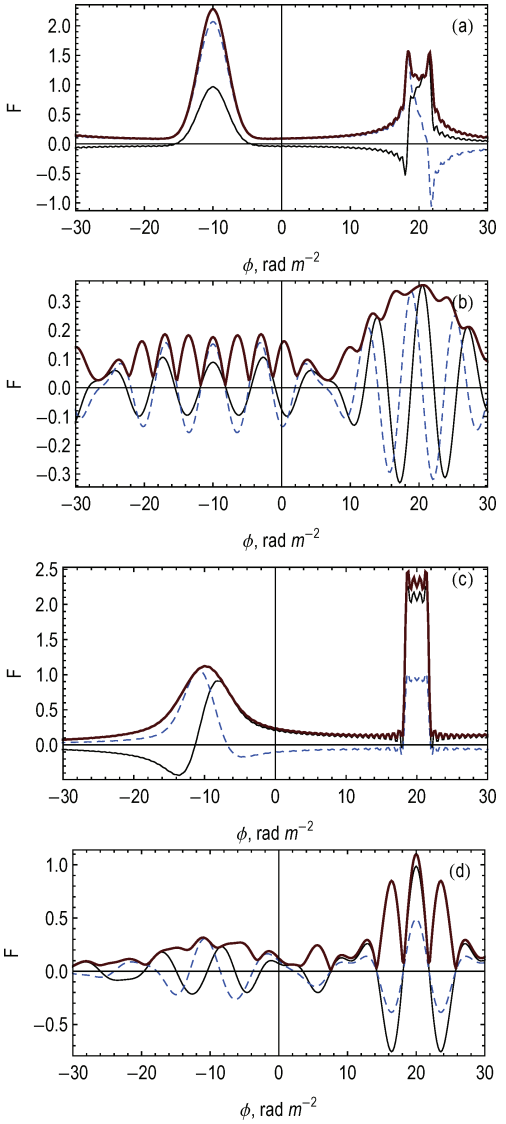

Figure 3. RM Synthesis for the test from Fig. 2 using the extension of $P(\lambda^2)$ in the domain $\lambda^2 < 0$ defined by (7). The parameter ϕ_0 is adjusted to the position of the left structure (a and b) or right structure (c and d). The whole domain of λ is used in panels (a and c) and the spectral window $0.6 < \lambda < 0.78$ m in panels (b and d). Real part – thin solid, imaginary part – dashed, amplitude – thick solid.

occur in each layer, but is obviously incorrect. In the same figure, we show the result of $F(\phi)$ reconstruction within the spectral band $0.6 < \lambda < 0.78$ m (panel c). Then both structures become diffuse with a more or less arbitrary phase. The last panel illustrates what happens if the upper wavelength boundary will be extended up to $\lambda = 2.5$ m (as expected for the Low Frequency Array and the Square Kilometre Array telescopes). This extension essentially improves the recognition of the sharp structure (the right one in the figure) but almost does not affect the reconstruction of the left (Gaussian) structure.

To avoid the non-uniqueness in the Faraday dispersion function reconstruction, some additional information (or hypothesis) is required. We suggest to improve the above reconstruction by some constraint concerning the possible symmetry of an isolated object.

Suppose that the expected objects are mainly galactic discs with magnetic fields believed to be symmetric with respect to the galactic equator. Then the desired F should be symmetric even with respect to the centre of the given object. Therefore, we consider each maximum of the reconstructed $F(\phi)$ separately and prescribe that the continuation of $P(\lambda^2)$ to the region of $\lambda^2 < 0$ has to be chosen in a way which makes $F(\phi)$ symmetric with respect to the point $\phi = \phi_0$, where ϕ_0 is the position of the maximum under consideration. This means that $F(2\phi_0 - \phi) = F(\phi)$ and using the shift theorem one gets

$$P(-\lambda^2) = \exp(-4\mathrm{i}\phi_0\lambda^2)P(\lambda^2). \quad (7)$$

The antisymmetric case can be considered as well with slight change in the algorithm: equation (7) changes to $P(-\lambda^2) = -\exp(-4\mathrm{i}\phi_0\lambda^2)P(\lambda^2)$.

Fig. 3 shows the results of reconstruction of the same test but following the suggested continuation. The test function includes two objects, while the algorithm includes only one parameter ϕ_0.

First, we performed the continuation adjusting ϕ_0 to the position of the left object (panel a). Then the method gives realistic result for this object. The reconstructed structure has no apparent internal field reversal and the ratio of real and imaginary parts of $F(\phi)$, i.e. the phase, is correctly reproduced. Position angles are restored with the accuracy of 3°. Of course, the result for the other layer, i.e. the second maximum of $|F(\phi)|$ in Fig. 3 remains false. Panel (b) shows what happens if the range of λ covered by the observation is reduced to $0.6 < \lambda < 0.78$ m. Instead of one peak one gets a sequence of peaks, which is a usual result for a Fourier reconstruction using a narrow spectral window. The suggested procedure does not suppress the sidelobes in the standard rotation measure spread function (RMSF) (Heald et al. 2009) but corrects the phase within the main central peak. Of course, the amplitude of each peak is much less than the amplitude of the peak in panel (a); however, the ratio of real and imaginary parts of $F(\phi)$ in the central peak remains realistic. If the parameter ϕ_0 is chosen following the position of the second object, the method gives a correct reconstruction for the right layer and fails to reproduce the left one. An obvious shortcoming of the method exploited is its local nature: We obtain a realistic shape of a chosen maximum and ignore what happens with the other one. A natural extension is to apply the recommendation of equation (7) locally to each maximum. This extension brings the idea of wavelets into consideration.

3 RM SYNTHESIS AND WAVELETS

Wavelet transform presents a kind of 'local' Fourier transform, allowing us to isolate a given structure in physical space and the Fourier space. Let us define the wavelet transform of the Faraday dispersion function $F(\phi)$ as

$$w_{\rm F}(a,b) = \frac{1}{|a|}\int_{-\infty}^{\infty} F(\phi)\psi^*\left(\frac{\phi-b}{a}\right)\mathrm{d}\phi, \tag{8}$$

where $\psi(\phi)$ is the analysing wavelet, a defines the scale and b defines the position of the wavelet. Then the coefficient $w_{\rm F}$ gives the contribution of corresponding structure into the function F.

The function F can be reconstructed using the inverse transform (see, e.g. Daubechies 1992)

$$F(\phi) = \frac{1}{C_\psi}\int_{-\infty}^{\infty}\int_{-\infty}^{\infty}\psi\left(\frac{\phi-b}{a}\right) w_{\rm F}(a,b)\,\frac{\mathrm{d}a\,\mathrm{d}b}{a^2}. \tag{9}$$

The reconstruction formula (9) exists under condition that

$$C_\psi = \frac{1}{2}\int_{-\infty}^{\infty}\frac{|\hat{\psi}(k)|^2}{|k|}\mathrm{d}k < \infty. \tag{10}$$

Here $\hat{\psi}(k) = \int \psi(\phi)\mathrm{e}^{-\mathrm{i}k\phi}\mathrm{d}\phi$ is the Fourier transform of the analysing wavelet $\psi(\phi)$.

Let us emphasize that the inverse formula (9) is usually written for real signals. Then the scale parameter a is positively defined and the integral is taken for $0 < a < \infty$. In the case of a complex-valued function, the range of a can be limited by positive values $a > 0$ by taking a *real* analysing wavelet $\psi(x)$. In general case of a complex-valued function and a complex wavelet, the scale parameter a should be extended into the domain of negative values (like wavenumbers in Fourier space).

For the sake of definiteness, we use as the analysing wavelet the so-called Mexican hat $\psi(\phi) = (1-\phi^2)\exp(-\phi^2/2)$. The wavelet is real, however, the function P is complex, so that the wavelet coefficients $w_{\rm F}$ are complex as well. For the chosen wavelet $w_{\rm F}(-a, b) = w_{\rm F}(a, b)$ and $C_\psi = 1$.

Using the definition of the wavelet transform (8) and relation (3) we can directly define the wavelet decomposition of the Faraday dispersion function from the polarized intensity $P(\lambda^2)$

$$w_{\rm F}(a,b) = \frac{1}{\pi}\int_{-\infty}^{\infty} P(\lambda^2)\mathrm{e}^{-2\mathrm{i}b\lambda^2}\hat{\psi}^*(-2a\lambda^2)\mathrm{d}\lambda^2. \tag{11}$$

Note that in the case of real F the problem of negative λ^2 can be solved using progressive wavelets, whose Fourier image is localized in the domain of positive wavenumbers. Thus, using this kind of wavelets one avoids the problem of the $P(\lambda^2)$ continuation in the domain $\lambda^2 < 0$.

For the general case, we divide Equation (11) into two parts $w_{\rm F}(a, b) = w_-(a, b) + w_+(a, b)$, where

$$w_-(a,b) = \frac{1}{\pi}\int_{-\infty}^{0} P(\lambda^2)\mathrm{e}^{-2\mathrm{i}b\lambda^2}\hat{\psi}^*(-2a\lambda^2)\mathrm{d}\lambda^2, \tag{12}$$

$$w_+(a,b) = \frac{1}{\pi}\int_{0}^{\infty} P(\lambda^2)\mathrm{e}^{-2\mathrm{i}b\lambda^2}\hat{\psi}^*(-2a\lambda^2)\mathrm{d}\lambda^2. \tag{13}$$

We propose the following algorithm: first, knowing $P(\lambda^2)$ for $\lambda^2 > 0$ we calculate the coefficients $w_+(a, b)$ and we recognize the dominating structures in the map $|w_+(a, b)|$. The coordinate b of the corresponding maximum gives us the value of ϕ_0^i, where upper index i indicates the number of the structure. Then we reconstruct the coefficients $w_-(a, b)$ following the idea of equation (7), but reformulated for the local domain in wavelet space (a, b). Namely, we define

$$w_-(a,b) = w_+\left[a, 2\phi_0^i(a,b) - b\right], \tag{14}$$

where the parameter $\phi_0^i(a, b)$ for the given point (a, b) is chosen according to the structure i which dominates in its vicinity.

Now we apply the suggested algorithm to the test function from Fig. 2. The map $|w_+(a, b)|$ presented in Fig. 4a demonstrates two well-defined structures. The b coordinates of the maxima are taken as ϕ_0^i. The result of the reconstruction (see Fig. 4b) shows that the method reproduces the amplitude and phase of $F(\phi)$ for both layers. The reconstruction here is performed using $P(\lambda^2)$ for the whole range $\lambda^2 > 0$. The comparison of the reconstructed position angle using standard and wavelet-based RM Synthesis is shown in Fig. 5. The suggested algorithm gives correct value for χ within both emission regions. Panels (c) and (d) show what happens for the reconstruction using the spectral window $0.6 < \lambda < 0.78$ m. One can see the wavelet map is empty in its substantial part $a > 2$; however, the structures remain well recognizable (panel c). The reconstructed F contains several oscillations in domains related to both layers. The amplitude of each oscillation becomes much lower than that in panel (b); however, the ratio of the real and imaginary parts in the central maxima remains correct. The third couple of panels shows the reconstruction within the extended window $0.6 < \lambda < 2.5$ m. This extension allows one to keep the horn-like structures in the bottom of the wavelet plane (panel e) which provide the reconstruction of sharp boundaries of the box-like structure (panel f).

4 CONCLUSIONS

The development of multichannel observations of polarized radio emission opens promising perspectives for the understanding of cosmic magnetic fields on galactic and intergalactic scales. The

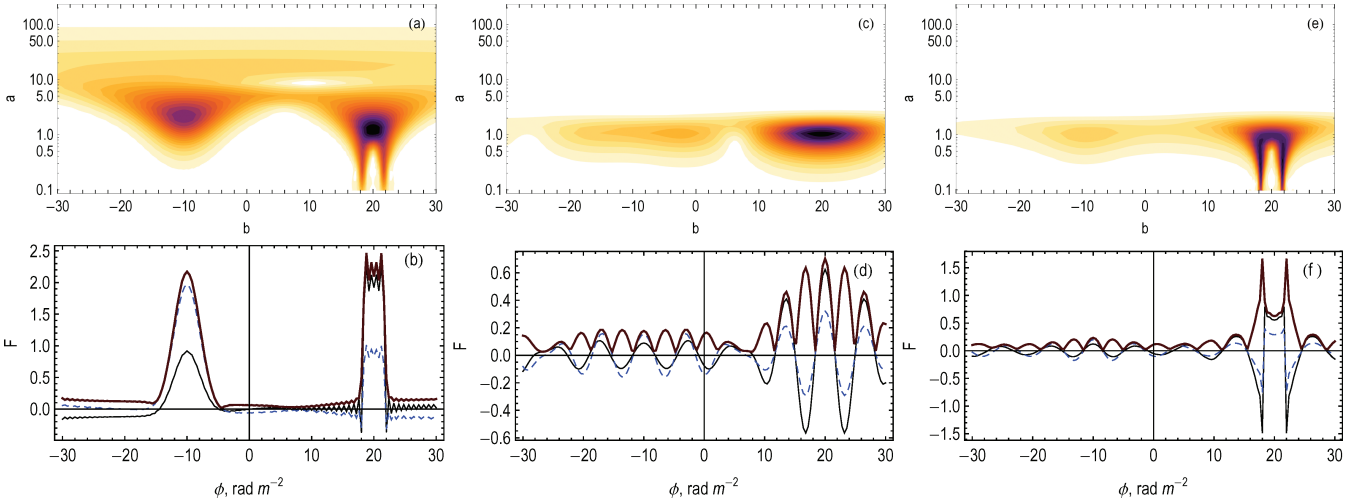

Figure 4. Wavelet-based RM Synthesis for the test from Fig. 2. The modulus of wavelet coefficients on the (a, b) plane (panels a, c and e) and the result of reconstruction (panels b, d and f) for whole domain of λ (panels a and b) and the windows $0.6 < \lambda < 0.78$ m (panels c and d) and $0.6 < \lambda < 2.5$ m (panels e and f). Real part – thin solid, imaginary part – dashed, amplitude – thick solid.

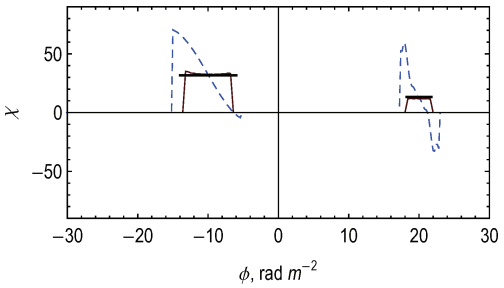

Figure 5. The intrinsic position angle χ for the test from Fig. 2(a) has been reconstructed with standard (dashed) and wavelet-based (thin solid) RM Synthesis. The whole domain of λ is used. Thick solid lines show initial χ in the location of the both structures.

first fruitful applications of RM Synthesis suggested in this context include the recognition of local structures in the Milky Way (Haverkorn et al. 2003), clusters of galaxies (de Bruyn & Brentjens 2005) and spiral galaxies (Heald et al. 2009). However, in general the RM Synthesis algorithm contains a fundamental problem emerging from the fact that the reconstruction formula requires the definition of complex polarized intensity in the range $-\infty < \lambda^2 < \infty$. In this Letter, we introduce a simple method for continuation of observed complex polarized intensity $P(\lambda^2)$ into the domain of negative $\lambda^2 < 0$. The method is suggested in context of magnetic field recognition in galactic discs, for which the magnetic field strength is supposed to have a maximum in the equatorial plane.

The suggested method is quite simple when applied to a single structure on the line of sight. Recognition of several structures on the same line of sight requires a more sophisticated technique. The problem of structure separation is resolved using the wavelet decomposition. A simple test example demonstrates the applicability of this method. The polarization angle reconstruction is significantly improved over the standard technique. The wavelets can be useful to also overcome some other problems of RM Synthesis, related to the multiband structure of the observational domain in λ-space, noise filtration, etc (e.g. Frick et al. 1997, 2001). The method essentially improves the possibilities for reconstruction of complicated Faraday structures using the capabilities of modern radio telescopes.

Finally, note that our simple examples illustrate that the extension of the observational band into the long-wavelength domain is helpful for the recognition of structures with sharp boundaries, while the short-wavelength domain is crucial for the reconstruction of smooth structures.

ACKNOWLEDGMENTS

This work was supported by the DFG-RFBR grant 08-02-92881.

REFERENCES

Beck R., 2009, Rev. Mex. Astron. Astrofis., 36, 1
Brentjens M. A., de Bruyn A. G., 2005, A&A, 441, 1217
Burn B. J., 1966, MNRAS, 133, 67
Daubechies I., 1992, Applied Math., 61
de Bruyn A. G., Brentjens M. A., 2005, A&A, 441, 931
Frick P., Baliunas S. L., Galyagin D., Sokoloff D., Soon W., 1997, ApJ, 483, 426
Frick P., Beck R., Berkhuijsen E. M., Patrickeyev I., 2001, MNRAS, 327, 1145
Haverkorn M., Katgert P., de Bruyn A. G., 2000, A&A, 356, L13
Haverkorn M., Katgert P., de Bruyn A. G., 2003, A&A, 403, 1031
Heald G., Braun R., Edmonds R., 2009, A&A, 503, 409
Sokoloff D. D., Bykov A. A., Shukurov A., Berkhuijsen E. M., Beck R., Poezd A. D., 1998, MNRAS, 299, 189

This paper has been typeset from a TEX/LATEX file prepared by the author.